ACS Energy LETTERS

Cite This: ACS Energy Lett. 2018, 3, 735−741

LETTER

Delocalization Drives Free Charge Generation in Conjugated Polymer Films

Natalie A. Pace,[†,‡] Obadiah G. Reid,[†,§] and Garry Rumbles*[,†,‡,§]

[†]National Renewable Energy Laboratory, 15013 Denver West Parkway, Golden, Colorado 80401, United States
[‡]Department of Chemistry and Biochemistry, University of Colorado Boulder, Boulder, Colorado 80309, United States
[§]Renewable and Sustainable Energy Institute, University of Colorado Boulder, Boulder, Colorado 80309, United States

Supporting Information

ABSTRACT: We demonstrate that the product of photoinduced electron transfer between a conjugated polymer host and a dilute molecular sensitizer is controlled by the structural state of the polymer. Ordered semicrystalline solids exhibit free charge generation, while disordered polymers in the melt phase do not. We use photoluminescence (PL) and time-resolved microwave conductivity (TRMC) measurements to sweep through polymer melt transitions in situ. Free charge generation measured by TRMC turns off upon melting, whereas PL quenching of the molecular sensitizers remains constant, implying unchanged electron transfer efficiency. The key difference is the intermolecular order of the polymer host in the solid state compared to the melt. We propose that this order−disorder transition modulates the localization length of the initial charge-transfer state, which controls the probability of free charge formation.

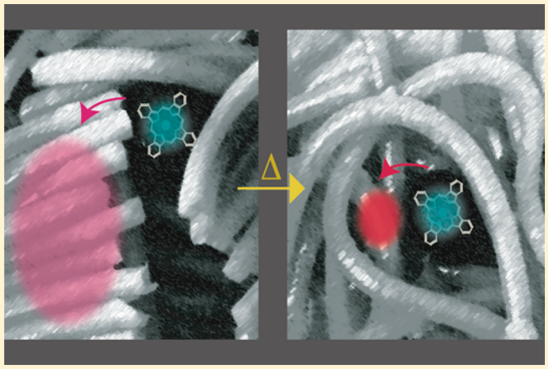

Photoinduced electron transfer depends on three crucial parameters according to the Marcus formulation: the electronic coupling (J_{DA}) between donor (D) and acceptor (A), the available driving force (ΔG_{CT}), and the reorganization energy of each molecule ($\lambda_{D,A}$).[1] Numerous studies have explored and validated this understanding in solution-phase systems,[2−4] but intermolecular electron transfer in solid-state systems is less well-understood. We have found that Marcus theory qualitiatively applies to certain solid organic donor/acceptor (D/A) systems,[5,6] but there is an additional layer of complexity that remains to be explained: what controls whether electron transfer results in free mobile charges or Coulombically bound charge-transfer (CT) states? The former can be used to do work in an electrochemical or photovoltaic cell. The latter will recombine.

Onsager theory predicts only bound charges when the dielectric constant of the medium is low (ε_r = 3−4), as is the case in organic solids.[7] Nevertheless, photoinduced electron transfer in solid-state D/A mixtures often results in long-lived (0.1−1 μs) free charges that are produced on an ultrafast time scale (0.1−1 ps) at near-unity efficiency.[7−12] This presents an interesting contrast with what is found for covalently bound D/A complexes in low-dielectric solvents, where photoinduced electron transfer yields an initial so-called charge-separated (CS) state that forms on a slower time scale (1−100 ps), with a faster associated recombination process (50−100 ns) than in the solid state.[13−16] Clearly, the CS state in the D/A molecule remains bound and differs from the free charges generated in the solid state; the significant difference in time scales noted above for both charge separation and recombination between solid-state and solution-phase D/A systems indicates that the mechanism of free charge generation is different from that of CS state formation. Understanding this difference is the key scientific question that is addressed here.

The ultrafast and efficient free-charge generation in solid-state D/A systems can be described by a quantum coherent model of charge transfer, where the initial CT state is delocalized over coupled intermolecular aggregates. Forward transfer occurs coherently, followed by rapid collapse into localized polarons with a large average initial separation (3−4 nm). Thus, the charges avoid coulomb capture[17,18] while ensuring that recombination must occur through slow incoherent hopping. This so-called "quantum ratchet" model[19] depends on a finely balanced interplay of coherent and incoherent evolution, much of which is beyond the scope of this Letter to test. While we cannot directly probe coherent transfer dynamics, the model ultimately rests on a simple, readily testable parameter: intermolecular electronic coupling between neighboring donor or acceptor units. Indeed, the

Received: January 22, 2018
Accepted: February 19, 2018
Published: February 19, 2018

DOI: 10.1021/acsenergylett.8b00108
ACS Energy Lett. 2018, 3, 735−741

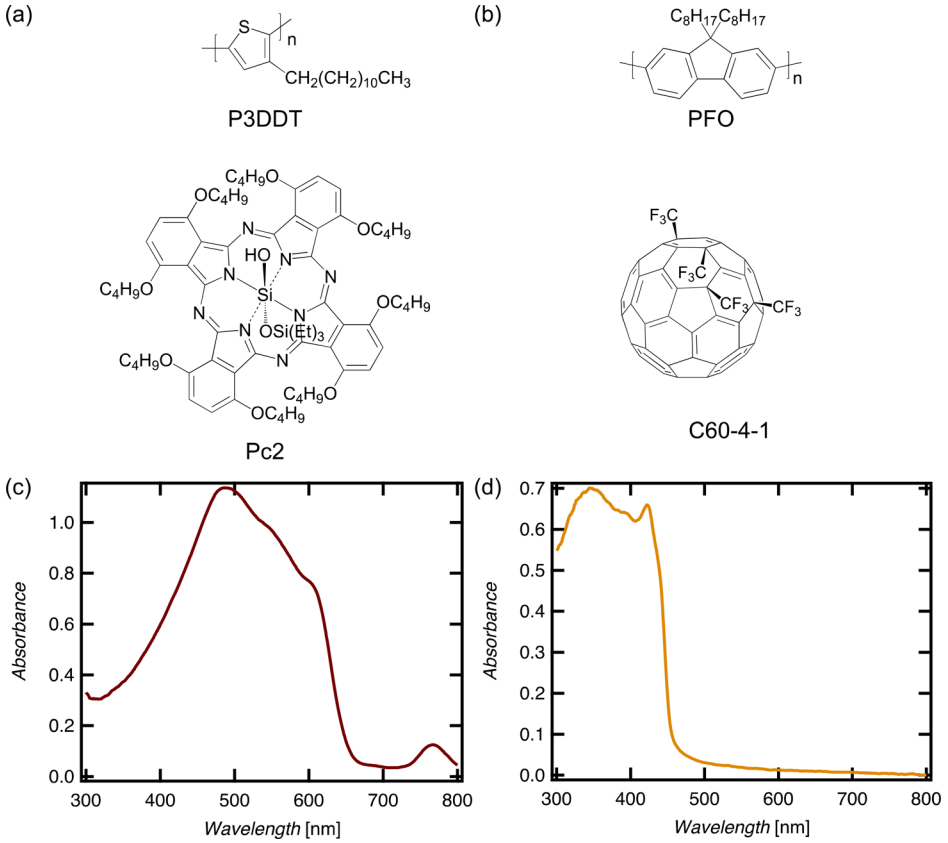

Figure 1. (a) Model system 1: P3DDT and Pc2 structures. (b) Model system 2: PFO and C60-4-1 structures. (c) Absorption spectrum of the P3DDT/Pc2 sensitized system. (d) Absorption spectrum of the PFO/C60-4-1 sensitized system.

"quantum ratchet" model has been supported by a variety of concentration-dependent studies, where increased acceptor concentrations associated with aggregate formation have been linked to increased charge generation efficiency.[8,20,21] Enhanced intermolecular coupling in both donor[10,22] and acceptor[23,24] components has also been associated with more efficient free charge generation. In this case, intermolecular coupling refers to the coupling between donor or acceptor chromophores and is not the same as the coupling between donor and acceptor (J_{DA}). Even in neat polymers, the presence of ordered crystalline regions has been shown to enhance free charge generation, while crystallite size controls the charge carrier lifetime.[25−28]

We are not aware of significant counter examples to this trend. Early work on high-performance low band gap copolymers (which make efficient organic solar cells and/or transistors) initially suggested that these materials were amorphous, but more recent studies using synchrotron X-ray diffraction and absorption measurements,[29,30] as well as high-resolution transmission electron microscopy,[31,32] have found significant order. Semicrystalline or para-crystalline order in conjugated polymers is not exceptional: it is ubiquitous, and it is extremely challenging to eliminate if one wishes to study a truly amorphous system.

The unique feature of the work we report here is that we are able to *switch* the degree of order in a conjugated polymer film from semicrystalline to amorphous and monitor the effect this has on electron transfer and free charge generation while keeping the other relevant parameters (J_{DA}, ΔG_{CT}, and $\lambda_{D,A}$) approximately constant. Small changes in these three parameters cannot be completely eliminated, but we show through control experiments that the rate of electron transfer is not strongly affected by the order−disorder transition. This provides a direct test of the role of intermolecular order in free charge generation.

We use two disparate polythiophene and polyfluorene polymers in our model systems, along with both fullerene and phthalocyanine acceptors. Temperature-dependent time-resolved microwave conductivity (TRMC)[21,33] is used to induce and monitor an order−disorder transition from a semicrystalline solid phase to a disordered melt within a single sample. Because TRMC is a contactless technique, the complexities of device fabrication are avoided, and we are able to use ultralow sensitizer (acceptor) concentrations to eliminate the effects of acceptor aggregation on charge generation efficiency. This has the added benefit of trapping the electron on the sensitizing molecule, such that the microwave probe is sensitive only to mobile holes in the donor polymers. We use in situ photoluminescence (PL) measurements to characterize the polymer phase as a function of temperature as well as evaluate the degree of PL quenching in the sensitizing molecules. We are therefore able to observe changes in charge transfer efficiency, free charge generation, and molecular structure simultaneously.

We examine poly(3-dodecylthiophene-2,5-diyl) (P3DDT) and a substituted silicon phthalocyanine (Pc2) (molecule 2 in ref 34) as our first model system (Figure 1a) and poly(9,9'-dioctylfluorene) (PFO) and C_{60} substituted with four trifluoromethyl groups (C60-4-1)[35] as our second system (Figure 1b). PFO and P3DDT have dramatically different microstructure, where P3DDT forms whiskerlike crystallites driven by a chain-folding process,[36] while PFO forms many

DOI: 10.1021/acsenergylett.8b00108
ACS Energy Lett. 2018, 3, 735−741

different types of crystallites, including a primary α crystallite phase and a metastable α' phase.[37,38] These two polymers thus offer a relatively diverse sampling of polymer environments. Both polymers have the added benefit of extensive optical and morphological study, such that changes in PL spectra can be linked to expected structural changes. We chose the first donor/acceptor pairing based on our previous finding that regioregular poly(3-hexylthiophene-2,5-diyl) (RR-P3HT) and Pc2 efficiently generate free charges on a femtosecond time scale.[22] We use a polythiophene derivative with dodecyl side chains for its substantially lower melting point of ∼450 K (relative to ∼570 K for RR-P3HT),[36] which is within the range of temperatures accessible by our cryostat. We chose the second system based on our previous finding that this particular polyfluorene/fullerene sensitized system is optimal for charge generation at subaggregation concentrations in PFO.[5] PFO also has a relatively low melting point of ∼430−440 K.[37,39]

Both model systems have well-separated absorption profiles, which allow for selective excitation of the donor or acceptor species. As shown in Figure 1c, the band edge of P3DDT lies at ∼605 nm, while the Q-band of the Pc2 absorption spectrum is peaked at ∼765 nm. As shown in Figure 1d, the band edge of PFO lies at ∼436 nm. The extinction coefficient and concentration of C60-4-1 are low, but previous measurements in solution reveal an absorption edge of ∼680 nm.[35] Both small molecules are dispersed at a concentration (molality) of 0.004 m in the polymer hosts. We use the same molality in both model systems in order to keep the mass of polymer "solvent" constant across differing repeat unit molecular weights.

We use these ultralow acceptor concentrations for three reasons. First, we eliminate the effects of acceptor aggregation on charge generation. This allows us to focus on the molecular order of only the donor polymer. Second, we eliminate the contribution of the acceptor species to the photoconductance signal, which we present as the product of charge carrier yield and the sum of contributing mobility components, $\phi\Sigma\mu$.[21] If the electron mobility is eliminated, this sum is simplified to $\phi\cdot\mu_{hole}$. Third, when combined with selective excitation of the acceptor species, this eliminates the impact of exciton diffusion on charge transfer dynamics as a function of temperature and microstructure. As a result of these three considerations, we effectively isolate free charge generation dynamics in our measurements, as reported by the mobility of only the hole in the polymer phase, while the PL quenching of the dilute sensitizer reports the efficacy of charge transfer, independent of whether the product is free charges or a CT state. We note that in all cases, the acceptor molecule possesses the lowest-energy singlet excited state in the system, and quenching due to energy transfer is not possible upon acceptor excitation.

For each sample, we simultaneously measure the photoconductance transient and the PL spectrum as a function of temperature. We selectively excite P3DDT at 450 nm in order to track changes in polymer morphology through the thermochromism of the emission spectrum, and we selectively excite Pc2 at 750 nm in order to detect changes in interfacial charge dynamics. We use these excitation conditions to simplify experimental interpretation as previously discussed, and we use Pc2 for its large extinction coefficient. However, we observe analogous charge generation behavior as a function of temperature upon 450 nm excitation while using $PC_{71}BM$ as an acceptor molecule (Figures S1 and S2). Both PL and TRMC measurements are made on the same sample in situ at each temperature.

As shown in Figure 2a, the P3DDT PL spectrum shows little evolution below the melting point (∼450 K), between 300 and

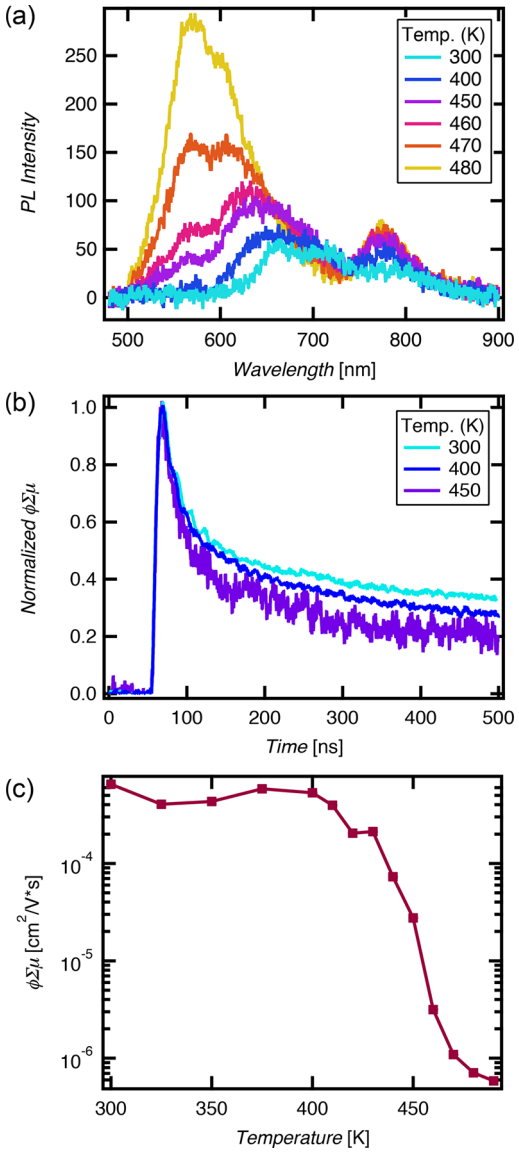

Figure 2. P3DDT/Pc2 (a) PL spectra as a function of temperature (450 nm excitation). (b) Normalized representative TRMC transients (750 nm excitation). (c) $\phi\Sigma\mu$ (t = 0) values as a function of temperature

400 K. There is a small peak at ∼780 nm from energy transfer to Pc2, which increases in intensity by small amounts as the P3DDT quantum yield of fluorescence increases. Between 300 and 400 K, there is only a subtle decrease in the average lifetime of the TRMC transient (Figure 2b) and a slight decrease of the initial yield mobility product determined from fits of the transients (Figures 2c and S3).

In contrast, between 400 and 480 K, where the melt transition occurs, there is a substantial blue shift and change in the shape of the polymer PL spectrum, which has previously been attributed to a direct transition between the crystalline phase of P3DDT and the amorphous melt phase via differential scanning calorimetry (DSC) and X-ray diffraction (XRD).[40] The $\phi\Sigma\mu$ value simultaneously drops by more than 2 orders of magnitude. Above the melt, the TRMC signal is essentially zero

DOI: 10.1021/acsenergylett.8b00108
ACS Energy Lett. 2018, 3, 735−741

(Figure S4). As previously mentioned, this value can be simplified to $\phi \cdot \mu_{hole}$ given the small concentration of acceptor molecules. However, we attribute this precipitous drop in signal primarily to ϕ_{hole}, because polymers exhibit similarly high GHz-frequency charge carrier mobility in the melt phase and in solution as they do in room-temperature thin films.[41,42] Indeed, the mobility in solution is generally higher than in thin films. This is because the GHz-frequency mobility in conjugated polymers is primarily determined by intrachain transport[43] and thus is not significantly affected by large changes in morphology in the solid state.[44]

Interestingly, before yields become vanishingly small, $\varphi\Sigma\mu$ below 10^{-6}, the average lifetime of the transients continues to subtly decrease with temperature. The mismatch between the relatively small changes in lifetime and the large changes in overall yield suggest that the fundamental free charge generation mechanism remains the same, even as the number of sites appropriate for free charge generation decreases.

In order to determine whether charge transfer turns off upon melting the P3DDT/Pc2 sample, we quantitatively measure the amount of PL quenching in the Pc2 molecule at room temperature and at the melt temperature (Figure 3). We use a

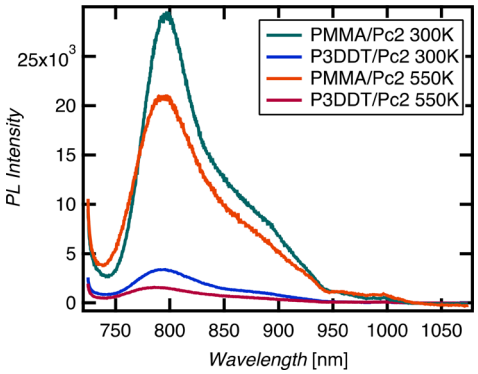

Figure 3. PL spectra of P3DDT/Pc2 and reference PMMA/Pc2 sample before and after the melting temperature of P3DDT. Excitation at 700 nm.

poly(methyl methacrylate) (PMMA) matrix with the same concentration of Pc2 molecules as a reference for 0% PL quenching from charge transfer. This reference sample also accounts for changes in nonradiative decay processes intrinsic to Pc2 as a function of temperature. We excite both samples at 700 nm under the same excitation and PL collection conditions. We find that when it is embedded in P3DDT, Pc2 PL is quenched by 87 ± 4% at 300 K and 92 ± 2% at 550 K.

Because the Pc2 PL is quenched by approximately the same amount both before and after the melting point of P3DDT, we conclude that charge transfer is equally efficient at both temperatures. Therefore, the parameters relevant to the initial charge transfer step (e.g., J_{DA}, ΔG_{CT}, and $\lambda_{D,A}$) remain relatively constant when the polymer is melted. However, before the melting point, charge transfer results in free charge generation, as evidenced by the large, long-lived TRMC signal. After the melt, charge transfer likely results in the formation of tightly bound CT states that decay nonradiatively, as evidenced by the disappearance of a TRMC signal but the persistence of PL quenching. This interpretation is corroborated by our previous study of semicrystalline RR-P3HT and "amorphous" regiorandom (RRa-) P3HT, where both sensitized systems with Pc2 produce a ground-state bleach in the polymer upon excitation of Pc2, but only the RR-P3HT system efficiently generates free charges probed by TRMC.[22] We show the same behavior in the acceptor phase, where low concentrations of $PC_{61}BM$ in RRa-P3HT yield significant RRa-P3HT PL quenching without an appreciable TRMC signal. As the concentration is increased, the PL quenching efficiency does not change significantly, but the TRMC signal rises because of free charge generation enabled by fullerene aggregation.

We generalize our results across different polymer microstructural environments through the examination of a PFO/C60-4-1 sensitized system. Similar to the P3DDT/Pc2 system, we selectively excite PFO at 415 nm in order to track morphological changes through the polymer emission spectrum, and we selectively excite C60-4-1 at 500 nm in order to detect changes in free charge generation through TRMC. In this case, we observe more distinct changes in the PL spectra and TRMC transients below the melting transition (~430−440 K), between 300 and 420 K (Figure 4). The PL spectrum at 300 K is dominated by the "β phase," which is a chain conformation defined by an intermonomer torsion angle of 180°.[39] This conformation is often associated with crystallite formation but can form apart from interchain interactions.[39] The corresponding photoconductance signal is large and long-lived, which may be a result of delocalization along a single chain in the β phase or delocalization via crystallites in the α' crystalline phase present at room temperature.

At 420 K, the PL spectrum is blue-shifted compared to room temperature and exhibits a vibrational progression characteristic of the α crystalline phase.[37] This is consistent with the previous finding that the α' phase reorganizes to the α phase above ~390 K, where the two phases are differentiated by slight changes in the length of the b crystallographic axis and the orientation of the a axis relative to the film surface.[37] This change in crystalline phase is accompanied by an increase in the $\phi\Sigma\mu$ value but a pronounced decrease in the average lifetime. In this case, the increase in $\phi\Sigma\mu$ is subtle and may be attributable to an increase in either ϕ_{hole} or μ_{hole} as a function of crystalline phase. The contribution from μ_{hole} may be more significant in this case, given the relatively small change in $\phi\Sigma\mu$ as well as the previous observation of an inverse correlation between carrier mobility and lifetime in organic blends.[45]

The PL spectrum after the melt transition (450 K) reflects the presence of a nematic phase,[37] which is an amorphous liquid crystalline phase with dampened, blue-shifted emission that is present in PFO up to ~570 K.[37,39] The photoconductance signal decreases concomitantly with the PL at the melting transition, ~440 K. Thus, we see that even though the microstructure of PFO varies significantly from that of P3DDT, and they contain different sensitizing molecules, they behave very similarly when crossing the melt transition. Both sensitized films exhibit free charge generation just below the melt transition, while just above it, neither film produces a photoconductance signal distinguishable from the instrument response.

In the case of PFO/C60-4-1, we are unable to use PL quenching of the C60-4-1 molecule (which has a very low PL quantum yield) to test whether electron transfer is equally efficient in the melt, as is the case for P3DDT/Pc2. However, given that the PFO/C60-4-1 system is at the optimal driving force for electron transfer,[5] it seems unlikely that it behaves differently in this respect. The driving force would have to change by more than 300 meV in order to reduce the electron transfer yield by half.[5]

DOI: 10.1021/acsenergylett.8b00108
ACS Energy Lett. 2018, 3, 735−741

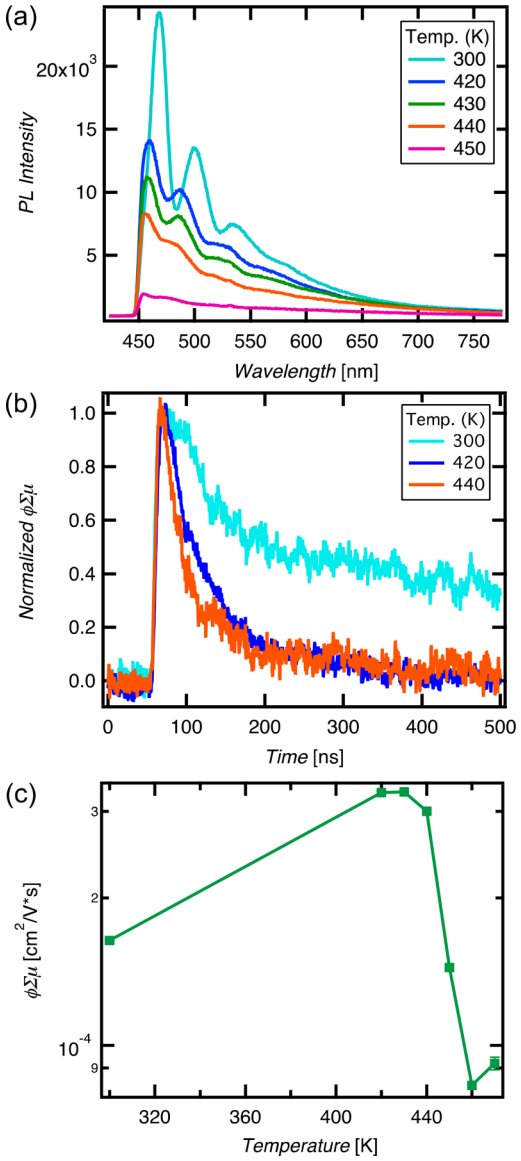

Figure 4. PFO/C60-4-1 (a) PL spectra as a function of temperature (415 nm excitation). (b) Normalized representative TRMC transients (500 nm excitation). (c) $\phi\Sigma\mu$ (t = 0) values as a function of temperature.

Our findings on these two chemically and physically distinct model systems are consistent with the "quantum ratchet" model described previously, where coherent charge transfer is supported by charge delocalization over coupled molecular domains. We find that intermolecular ordering is indeed a prerequisite for free charge generation. Photoinduced electron transfer occurs whether there is order or not, but in amorphous melts it does not produce mobile carriers that are detectable in our photoconductance experiments. This could be a result of short lifetimes (<100 ps) or low mobility in amorphous films. Likely it is both. We reiterate, however, that we do not think low-microwave frequency mobility is apt to be a fundamental property of conjugated polymer melts. Rather, mobilities likely decrease in the melt phase because charges are trapped by a deep coulomb potential at the molecular D/A interface.

We have studied the influence of intermolecular order on free charge generation in two different conjugated polymer donors (PFO and P3DDT) sensitized with a small concentration of electron-accepting molecules (Pc2, $PC_{71}BM$, or C60-4-1). The photoluminescence and photoconductance of all these samples were measured in situ as the temperature was scanned through the respective polymer melt transitions, inducing an order−disorder transition that has a profound effect on the product of charge transfer. The low concentration of acceptors ensures that electronically coupled aggregates of these molecules are not present and that the only source of intermolecular coupling is the conjugated polymer. Upon melting, all sources of intermolecular electronic coupling are removed, and we observe that the photoconductance signal vanishes despite evidence from the P3DDT/Pc2 system that charge transfer continues unabated. Our interpretation of these data is that free charge generation can occur only in the presence of electronically coupled molecular aggregates, consistent with a "quantum ratchet" model of free charge generation in organic D/As. This finding can be used as a design principle in all solid-state organic charge generation systems.

■ ASSOCIATED CONTENT

Supporting Information

The Supporting Information is available free of charge on the ACS Publications website at DOI: 10.1021/acsenergylett.8b00108.

P3DDT/PC71BM system, transient fits, TRMC signal above melting temperature, smooth function, experimental methods, and TRMC cryostat design (PDF)

■ AUTHOR INFORMATION

Corresponding Author

*E-mail: Garry.Rumbles@nrel.gov.

ORCID

Natalie A. Pace: 0000-0001-6553-9363

Obadiah G. Reid: 0000-0003-0646-3981

Garry Rumbles: 0000-0003-0776-1462

Notes

The authors declare no competing financial interest.

■ ACKNOWLEDGMENTS

We thank J. Bergkamp and D. Gust (Arizona State University) for the provision of the sample of phthalocyanine, Pc2. In addition, we thank B. Larson, S. Strauss, and O. Boltalina (Colorado State University) for providing the fullerene derivative, C60-4-1 sample. This work was funded by the Solar Photochemistry Program of the Division of Chemical Sciences, Geosciences, and Biosciences, Office of Basic Energy Sciences of the U.S. Department of Energy through Grant DE-AC36-08-GO28308 to NREL.

■ REFERENCES

(1) Marcus, R. A. On the Theory of Oxidation-Reduction Reactions Involving Electron Transfer. *J. Chem. Phys.* **1956**, *24*, 966−978.

(2) Miller, J. R.; Calcaterra, L. T.; Closs, G. L. Intramolecular Long-Distance Electron Transfer in Radical Anions. *J. Am. Chem. Soc.* **1984**, *106*, 3047−3049.

(3) Rehm, D.; Weller, A. Kinetics of Fluorescence Quenching by Electron and H-Atom Transfer. *Isr. J. Chem.* **1970**, *8*, 259−271.

(4) Hush, N. S.; Paddon-Row, M. N.; Cotsaris, E.; Oevering, H.; Verhoeven, J. W.; Heppener, M. Distance Dependence of Photo-induced Electron Transfer Through Non-Conjugated Bridges. *Chem. Phys. Lett.* **1985**, *117*, 8−11.

DOI: 10.1021/acsenergylett.8b00108
ACS Energy Lett. 2018, 3, 735−741

(5) Coffey, D. C.; Larson, B. W.; Hains, A. W.; Whitaker, J. B.; Kopidakis, N.; Boltalina, O. V.; Strauss, S. H.; Rumbles, G. An Optimal Driving Force for Converting Excitons Into Free Carriers in Excitonic Solar Cells. *J. Phys. Chem. C* **2012**, *116*, 8916−8923.
(6) Ihly, R.; Mistry, K. S.; Ferguson, A. J.; Clikeman, T. T.; Larson, B. W.; Reid, O.; Boltalina, O. V.; Strauss, S. H.; Rumbles, G.; Blackburn, J. L. Tuning the Driving Force for Exciton Dissociation in Single-Walled Carbon Nanotube Heterojunctions. *Nat. Chem.* **2016**, *8*, 603−609.
(7) Few, S.; Frost, J. M.; Nelson, J. Models of Charge Pair Generation in Organic Solar Cells. *Phys. Chem. Chem. Phys.* **2015**, *17*, 2311−2325.
(8) Gelinas, S.; Rao, A.; Kumar, A.; Smith, S. L.; Chin, A. W.; Clark, J.; van der Poll, T. S.; Bazan, G. C.; Friend, R. H. Ultrafast Long-Range Charge Separation in Organic Semiconductor Photovoltaic Diodes. *Science* **2014**, *343*, 512−516.
(9) Provencher, F.; Bérubé, N.; Parker, A. W.; Greetham, G. M.; Towrie, M.; Hellmann, C.; Cote, M.; Stingelin, N.; Silva, C.; Hayes, S. C. Direct Observation of Ultrafast Long-Range Charge Separation at Polymer−Fullerene Heterojunctions. *Nat. Commun.* **2014**, *5*, 4288.
(10) Herrmann, D.; Niesar, S.; Scharsich, C.; Kohler, A.; Stutzmann, M.; Riedle, E. Role of Structural Order and Excess Energy on Ultrafast Free Charge Generation in Hybrid Polythiophene/Si Photovoltaics Probed in Real Time by Near-Infrared Broadband Transient Absorption. *J. Am. Chem. Soc.* **2011**, *133*, 18220−18233.
(11) Zarrabi, N.; Burn, P. L.; Meredith, P.; Shaw, P. E. Acceptor and Excitation Density Dependence of the Ultrafast Polaron Absorption Signal in Donor−Acceptor Organic Solar Cell Blends. *J. Phys. Chem. Lett.* **2016**, *7*, 2640−2646.
(12) Xu, X.; Li, Z.; Zhang, W.; Meng, X.; Zou, X.; Di Carlo Rasi, D.; Ma, W.; Yartsev, A.; Andersson, M. R.; Janssen, R. A. J.; et al. 8.0% Efficient All-Polymer Solar Cells with High Photovoltage of 1.1 V and Internal Quantum Efficiency Near Unity. *Adv. Energy Mater.* **2018**, *8*, 1700908.
(13) Hartnett, P. E.; Mauck, C. M.; Harris, M. A.; Young, R. M.; Wu, Y.-L.; Marks, T. J.; Wasielewski, M. R. Influence of Anion Delocalization on Electron Transfer in a Covalent Porphyrin Donor−Perylenediimide Dimer Acceptor System. *J. Am. Chem. Soc.* **2017**, *139*, 749−756.
(14) Kuciauskas, D.; Liddell, P. A.; Lin, S.; Stone, S. G.; Moore, A. L.; Moore, T. A.; Gust, D. Photoinduced Electron Transfer in Carotenoporphyrin−Fullerene Triads: Temperature and Solvent Effects. *J. Phys. Chem. B* **2000**, *104*, 4307−4321.
(15) Garg, V.; Kodis, G.; Chachisvilis, M.; Hambourger, M.; Moore, A. L.; Moore, T. A.; Gust, D. Conformationally Constrained Macrocyclic Diporphyrin−Fullerene Artificial Photosynthetic Reaction Center. *J. Am. Chem. Soc.* **2011**, *133*, 2944−2954.
(16) Ortiz, M.; Cho, S.; Niklas, J.; Kim, S.; Poluektov, O. G.; Zhang, W.; Rumbles, G.; Park, J. Through-Space Ultrafast Photoinduced Electron Transfer Dynamics of a C_{70}-Encapsulated Bisporphyrin Covalent Organic Polyhedron in a Low-Dielectric Medium. *J. Am. Chem. Soc.* **2017**, *139*, 4286−4289.
(17) Chen, K.; Barker, A. J.; Reish, M. E.; Gordon, K. C.; Hodgkiss, J. M. Broadband Ultrafast Photoluminescence Spectroscopy Resolves Charge Photogeneration via Delocalized Hot Excitons in Polymer:-Fullerene Photovoltaic Blends. *J. Am. Chem. Soc.* **2013**, *135*, 18502−18512.
(18) Barker, A. J.; Chen, K.; Hodgkiss, J. M. Distance Distributions of Photogenerated Charge Pairs in Organic Photovoltaic Cells. *J. Am. Chem. Soc.* **2014**, *136*, 12018−12026.
(19) Scholes, G. D.; Fleming, G. R.; Chen, L. X.; Aspuru-Guzik, A.; Buchleitner, A.; Coker, D. F.; Engel, G. S.; van Grondelle, R.; Ishizaki, A.; Jonas, D. M.; et al. Using Coherence to Enhance Function in Chemical and Biophysical Systems. *Nature* **2017**, *543*, 647−656.
(20) Savoie, B. M.; Rao, A.; Bakulin, A. A.; Gelinas, S.; Movaghar, B.; Friend, R. H.; Marks, T. J.; Ratner, M. A. Unequal Partnership: Asymmetric Roles of Polymeric Donor and Fullerene Acceptor in Generating Free Charge. *J. Am. Chem. Soc.* **2014**, *136*, 2876−2884.
(21) Savenije, T. J.; Ferguson, A. J.; Kopidakis, N.; Rumbles, G. Revealing the Dynamics of Charge Carriers in Polymer:Fullerene Blends Using Photoinduced Time-Resolved Microwave Conductivity. *J. Phys. Chem. C* **2013**, *117*, 24085−24103.
(22) Feier, H. M.; Reid, O. G.; Pace, N. A.; Park, J.; Bergkamp, J. J.; sellinger, A.; Gust, D.; Rumbles, G. Local Intermolecular Order Controls Photoinduced Charge Separation at Donor/Acceptor Interfaces in Organic Semiconductors. *Adv. Energy Mater.* **2016**, *6*, 1502176.
(23) Larson, B. W.; Reid, O. G.; Coffey, D. C.; Avdoshenko, S. M.; Popov, A. A.; Boltalina, O. V.; Strauss, S. H.; Kopidakis, N.; Rumbles, G. Inter-Fullerene Electronic Coupling Controls the Efficiency of Photoinduced Charge Generation in Organic Bulk Heterojunctions. *Adv. Energy Mater.* **2016**, *6*, 1601427.
(24) Jakowetz, A. C.; Böhm, M. L.; Zhang, J.; Sadhanala, A.; Huettner, S.; Bakulin, A. A.; Rao, A.; Friend, R. H. What Controls the Rate of Ultrafast Charge Transfer and Charge Separation Efficiency in Organic Photovoltaic Blends. *J. Am. Chem. Soc.* **2016**, *138*, 11672−11679.
(25) Silva, C.; Russell, D. M.; Dhoot, A. S.; Herz, L. M.; Daniel, C. M.; Greenham, N. C.; Arias, A. C.; Setayesh, S.; M llen, K.; Friend, R. H. Exciton and Polaron Dynamics in a Step-Ladder Polymeric Semiconductor: the Influence of Interchain Order. *J. Phys.: Condens. Matter* **2002**, *14*, 9803−9824.
(26) Reid, O. G.; Pensack, R. D.; Song, Y.; Scholes, G. D.; Rumbles, G. Charge Photogeneration in Neat Conjugated Polymers. *Chem. Mater.* **2014**, *26*, 561−575.
(27) Reid, O. G.; Malik, J. A. N.; Latini, G.; Dayal, S.; Kopidakis, N.; Silva, C.; Stingelin, N.; Rumbles, G. The Influence of Solid-State Microstructure on the Origin and Yield of Long-Lived Photogenerated Charge in Neat Semiconducting Polymers. *J. Polym. Sci., Part B: Polym. Phys.* **2012**, *50*, 27−37.
(28) Marsh, H. S.; Reid, O. G.; Barnes, G.; Heeney, M.; Stingelin, N.; Rumbles, G. Control of Polythiophene Film Microstructure and Charge Carrier Dynamics Through Crystallization Temperature. *J. Polym. Sci., Part B: Polym. Phys.* **2014**, *52*, 700−707.
(29) Noriega, R.; Rivnay, J.; Vandewal, K.; Koch, F. P. V.; Stingelin, N.; Smith, P.; Toney, M. F.; Salleo, A. A General Relationship Between Disorder, Aggregation and Charge Transport in Conjugated Polymers. *Nat. Mater.* **2013**, *12*, 1038−1044.
(30) Rivnay, J.; Toney, M. F.; Zheng, Y.; Kauvar, I. V.; Chen, Z.; Wagner, V.; Facchetti, A.; Salleo, A. Unconventional Face-on Texture and Exceptional in-Plane Order of a High Mobility N-Type Polymer. *Adv. Mater.* **2010**, *22*, 4359−4363.
(31) Takacs, C. J.; Treat, N. D.; Krämer, S.; Chen, Z.; Facchetti, A.; Chabinyc, M. L.; Heeger, A. J. Remarkable Order of a High-Performance Polymer. *Nano Lett.* **2013**, *13*, 2522−2527.
(32) Schulz, G. L.; Fischer, F. S. U.; Trefz, D.; Melnyk, A.; Hamidi-Sakr, A.; Brinkmann, M.; Andrienko, D.; Ludwigs, S. The PCPDTBT Family: Correlations Between Chemical Structure, Polymorphism, and Device Performance. *Macromolecules* **2017**, *50*, 1402−1414.
(33) Reid, O. G.; Moore, D. T.; Li, Z.; Zhao, D.; Yan, Y.; Zhu, K.; Rumbles, G. Quantitative Analysis of Time-Resolved Microwave Conductivity Data. *J. Phys. D: Appl. Phys.* **2017**, *50*, 493002.
(34) Bergkamp, J. J.; Sherman, B. D.; Marino-Ochoa, E.; Palacios, R. E.; Cosa, G.; Moore, T. A.; Gust, D.; Moore, A. L. Synthesis and Characterization of Silicon Phthalocyanines Bearing Axial Phenoxyl Groups for Attachment to Semiconducting Metal Oxides. *J. Porphyrins Phthalocyanines* **2011**, *15*, 943−950.
(35) Park, J.; Ramirez, J. J.; Clikeman, T. T.; Larson, B. W.; Boltalina, O. V.; Strauss, S. H.; Rumbles, G. Variation of Excited-state Dynamics in Trifluoromethyl functionalized C_{60} Fullerenes. *Phys. Chem. Chem. Phys.* **2016**, *18*, 22937−22945.
(36) Malik, S.; Nandi, A. K. Crystallization Mechanism of Regioregular Poly(3-Alkyl Thiophene)S. *J. Polym. Sci., Part B: Polym. Phys.* **2002**, *40*, 2073−2085.
(37) Chen, S. H.; Su, A. C.; Su, C. H.; Chen, S. A. Crystalline Forms and Emission Behavior of Poly(9,9-di- n-octyl-2,7-fluorene). *Macromolecules* **2005**, *38*, 379−385.

DOI: 10.1021/acsenergylett.8b00108
ACS Energy Lett. 2018, 3, 735−741

(38) Scherf, U.; Neher, D. *Polyfluorenes*; Springer Verlag: Berlin, 2008.
(39) Perevedentsev, A.; Stavrinou, P. N.; Smith, P.; Bradley, D. D. C. Solution-Crystallization and Related Phenomena in 9,9-Dialkyl-Fluorene Polymers. II. Influence of Side-Chain Structure. *J. Polym. Sci., Part B: Polym. Phys.* **2015**, *53*, 1492−1506.
(40) Yang, C.; Orfino, F. P.; Holdcroft, S. A Phenomenological Model for Predicting Thermochromism of Regioregular and Non-regioregular Poly(3-alkylthiophenes). *Macromolecules* **1996**, *29*, 6510−6517.
(41) Warman, J. M.; Gelinck, G. H.; Haas, M. P. de. The Mobility and Relaxation Kinetics of Charge Carriers in Molecular Materials Studied by Means of Pulse-Radiolysis Time-Resolved Microwave Conductivity: Dialkoxy-Substituted Phenylene-Vinylene Polymers. *J. Phys.: Condens. Matter* **2002**, *14*, 9935−9954.
(42) Grozema, F. C.; Siebbeles, L. D. A. Charge Mobilities in Conjugated Polymers Measured by Pulse Radiolysis Time-Resolved Microwave Conductivity: From Single Chains to Solids. *J. Phys. Chem. Lett.* **2011**, *2*, 2951−2958.
(43) Laquai, F.; Wegner, G.; Bassler, H. What Determines the Mobility of Charge Carriers in Conjugated Polymers? *Philos. Trans. R. Soc., A* **2007**, *365*, 1473−1487.
(44) O'Connor, B. T.; Reid, O. G.; Zhang, X.; Kline, R. J.; Richter, L. J.; Gundlach, D. J.; DeLongchamp, D. M.; Toney, M. F.; Kopidakis, N.; Rumbles, G. Morphological Origin of Charge Transport Anisotropy in Aligned Polythiophene Thin Films. *Adv. Funct. Mater.* **2014**, *24*, 3422−3431.
(45) Vijila, C.; Singh, S. P.; Williams, E.; Sonar, P.; Pivrikas, A.; Philippa, B.; White, R.; Naveen Kumar, E.; Gomathy Sandhya, S.; Gorelik, S.; et al. Relation Between Charge Carrier Mobility and Lifetime in Organic Photovoltaics. *J. Appl. Phys.* **2013**, *114*, 184503.

DOI: 10.1021/acsenergylett.8b00108
ACS Energy Lett. 2018, 3, 735−741